

Rotation Measure Variations and Reversals of Repeating FRBs in Massive Binary Systems

Z. Y. ZHAO,¹ G. Q. ZHANG,¹ F. Y. WANG,^{1,2} AND Z. G. DAI³

¹*School of Astronomy and Space Science, Nanjing University, Nanjing 210093, China*

²*Key Laboratory of Modern Astronomy and Astrophysics (Nanjing University), Ministry of Education, Nanjing 210093, China*

³*Department of Astronomy, School of Physical Sciences, University of Science and Technology of China, Hefei 230026, Anhui, China*

ABSTRACT

Recent observations discovered that some repeating fast radio bursts (FRBs) show complicated variations and reversals of Faraday rotation measures (RMs), indicating that the sources of these FRBs are embedded in a dynamically magnetized environment. One possible scenario is that repeating FRBs are generated by pulsars in binary systems, especially containing a high-mass companion with strong stellar outflows. Here, we study the RM variations caused by stellar winds, and a possible stellar disc. If the magnetic field is radial in the stellar wind, RM will not reverse except if the magnetic axis inclination angle is close to 90°. For the toroidal magnetic field in the wind, RM will reverse at the super conjunction. For the case of the toroidal field in the disc, the RM variations may have a multimodal and multiple reversal profile because the radio signals travel through different components of the disc during periastron passage. We also apply this model to FRB 20180916B. By assuming its 16.35-day period is from a slowly rotating or freely precessing magnetar, we find that the secular RM variation can be explained by the periastron passage of a magnetar in a massive binary system. In addition, the clumps in the stellar wind and disc can cause short time-scale (< 1 day) variations or reversals of RM. Therefore, long-term monitoring of RM variations can reveal the environments of repeating FRBs.

Keywords: Radio transient sources, Magnetar, Pulsars, Stellar winds, Be stars, High mass x-ray binary stars

1. INTRODUCTION

Fast radio bursts (FRBs) are extragalactic millisecond-duration radio transients with high brightness temperatures and large dispersion measures (DMs). FRBs were first discovered more than a decade ago by Lorimer et al. (2007) and we have known little about their physical origins (see reviews of Zhang 2020; Xiao et al. 2021; Petroff et al. 2022). At least some FRBs originate from magnetars since FRB 200428 was detected from the Galactic magnetar SGR J1935+2154 (Bochenek et al. 2020; CHIME/FRB Collaboration et al. 2020a). The magnetar or pulsar related models are proposed to interpret the origins of FRBs (Murase et al. 2016; Beloborodov 2017; Kashiyama & Murase 2017; Metzger et al. 2017; Wang & Yu 2017; Yang

& Zhang 2018; Metzger et al. 2019; Lu et al. 2020; Wang et al. 2020). However, for the repeating FRBs being active for several years, the rotation energy is insufficient. The pulsar should be highly magnetized and FRBs should be powered by the magnetic energy (Lyutikov 2017).

Except for the very few FRBs close to us, we cannot make detailed observations of their surrounding medium, which is crucial for diagnosing their origin. For cosmological FRBs, we can indirectly obtain information about their local environment or progenitors through their polarization, DM, Faraday rotation measure (RM), scintillation, and scattering. The differences in observed DMs and RMs of FRBs mean that there may be different origins or that they are all from magnetars but in different environments. The large ($\sim 10^5$ rad m⁻²) and decreasing RM of FRB 20121102A (Michilli et al. 2018; Hilmarsson et al. 2021) may be from the magnetar wind nebula (Margalit & Metzger 2018; Zhao et al. 2021), a pulsar near a supermassive black hole (SMBH, Zhang 2018; Katz 2021a; Yang et al. 2022b) or a hyper-accreting X-ray binary (Sridhar & Metzger 2022). The extreme DM of FRB 20190520B may be related to the host galaxy (Niu et al. 2022) or a young supernova remnant (SNR, Zhao & Wang 2021; Katz 2022).

The observed RM, especially the extremely large or evolving values, can better reflect the properties of the magnetized environment around the source. Recently, the RM variations or reversals have been observed for some FRBs, such as FRB 20201124A (Xu et al. 2022) and FRB 20190520B (Anna-Thomas et al. 2022; Dai et al. 2022). A similar RM evolution has been found through the periastron passage of PSR B1259–63/LS 2883 (e.g., Johnston et al. 1996, 2005). Wang et al. (2022a) has proposed that FRB 20201124A and FRB 20190520B may reside in a magnetar/Be star binary system. The fast-rotating Be star will form a decretion disc. RM is expected to be variable when the bursts interact with the disc. The RM reversals of FRB 20201124A and FRB 20190520B can be also naturally explained in this model.

More recently, the RM variations of FRB 20180916B have been reported (Mckinven et al. 2022). FRB 20180916B was first discovered by the Canadian Hydrogen Intensity Mapping Experiment (CHIME) telescope with a low RM of -114.6 ± 0.6 rad m⁻² (CHIME/FRB Collaboration et al. 2019). It was localized in a nearby massive spiral galaxy at $z = 0.0337 \pm 0.0002$ (Marcote et al. 2020). The following monitoring showed that the DM has very little variation (Nimmo et al. 2021; Pastor-Marazuela et al. 2021; Mckinven et al. 2022). The |RM| has a small and stochastic variation before 2021 April (Chawla et al. 2020; Pleunis et al. 2021; Mckinven et al. 2022), and has a secular decrease during 2021 April and 2021 December (Mckinven et al. 2022).

Besides the above secular DM and RM variations, short-time RM variations have been measured in a pulsar binary system PSR B1744–24A (Li et al. 2022). A turbulent medium or cloud in SNR has been proposed to explain the irregular RM variations (Yang et al. 2022b). There may be an inhomogeneous medium near the FRB source, and the relative motion between the source and the medium causes stochastic RM variations. From observations, stellar winds (Moffat & Robert 1994; Puls et al. 2006) or stellar discs (Chernyakova et al. 2021) are found to be clumpy (e.g., the short variability on keV/GeV light curve, see Apparao et al. 1991; Chernyakova et al. 2020, 2021). Here, we will estimate the stochastic RM variation from the clumpy stellar wind and disc.

In this work, we study the effects of stellar winds and discs on the observational properties of FRBs in a high mass X-ray binary (HMXB) or a high mass γ -ray binary (HMGB) (see Fig. 1). The motivations to consider FRBs originating in binary systems are as follows. First, Tendulkar et al. (2021) found that FRB 20180916B is 250 pc away from the nearest region of active star formation in its host galaxy. The inferred age of the source should be about a few million years to traverse the observed separation for the typical kick velocity of a pulsar, which is opposed to a young active magnetar born in core-collapse supernova. However,

the separation and the inferred age can be compatible with a highly magnetised neutron star in an HMXB or an HMGB. Second, similar RM variations and reversals of repeating FRBs have been observed both in repeating FRBs (Xu et al. 2022; Anna-Thomas et al. 2022; Dai et al. 2022) and a binary system containing a pulsar and a massive Be star (PSR B1259–63/LS 2883) (Johnston et al. 1996, 2005). Wang et al. (2022a) found that RM variations and reversals can be well understood in a magnetar/Be star binary system. Third, short-time RM variations have been measured in a pulsar binary system PSR B1744–24A (Li et al. 2022). Massive stars usually have strong stellar winds, which is not discussed in detail in previous works (Wang et al. 2022a; Yang et al. 2022b). More importantly, the interactions between the stellar wind and the pulsar wind will form a bow shock cavity, which will play an essential role in the orbital modulations of RM, DM, and the free-free absorption process. In addition to a polar wind, a decretion disc will be formed for some Oe/Be stars. However, the disc will be truncated due to the tidal torques from the pulsar (Reig 2011). Luckily, the tidal interactions can be neglected in an eccentric orbital (Okazaki et al. 2011). We will only discuss the DM and RM from the disc with a high eccentricity orbital for simplicity.

This letter is organized as follows. In Section 2, the wind interaction and the geometric description of the binary system are shown. Taking FRB 20180916B as an example, Section 3 gives the results of RM, DM, and free-free absorption process from the stellar wind and disc. The stochastic DM and RM variations caused by the clumps in the stellar wind and disc are given in Section 4. The DM and RM variations for other repeating FRBs and the possible origins of the persistent radio sources (PRSs) in a binary system are discussed briefly in Section 5. Finally, a summary is given in Section 6.

2. WIND INTERACTIONS

2.1. The stellar outflows

For a massive star, the mass-loss is important via an approximately isotropic stellar wind. The electron density of the stellar wind from the radial distance r is given by

$$n_w(r) = n_{w,0} \left(\frac{r}{R_\star} \right)^{-2}, \quad (1)$$

where $n_{w,0}$ is the number density at the stellar surface and R_\star is the radius of the star. The constant mass-loss rate \dot{M} and the assumption of the completely ionized wind is used in this work. In this case, $n_{w,0}$ can be written as $n_{w,0} = \dot{M}/4\pi R_\star^2 v_w(r) \mu_i m_p$, where $v_w(r) = v_{w,\infty}(1 - R_\star/r)$ is the wind velocity with $v_{w,\infty}$ being the terminal speed of the wind, μ_i is the mean ion molecular weight and m_p is the mass of protons. At a large distance ($r \gg R_\star$), the wind velocity is $v_w \simeq v_{w,\infty}$. The typical value of mass-loss rate and wind velocity for Be stars is found to be $10^{-11} - 10^{-8} M_\odot \text{ yr}^{-1}$ and $v_w \sim 10^8 \text{ cm s}^{-1}$ from observations (Snow 1981; Krtićka 2014). For typical stellar outflows with hydrogen abundance $X \sim 0.7$ (Dubus 2013), $\mu_i = 4/(1 + 3X) \simeq 1.29$. For some Oe/Be stars, the slow equatorial outflow will form a decretion disc. The disc usually has a vertical Gaussian density profile (Carciofi & Bjorkman 2006)

$$n_d(r_d, z_d) = n_{d,0} \left(\frac{r_d}{R_\star} \right)^{-\beta_d} \exp \left[-\frac{z_d^2}{2H^2(r_d)} \right], \quad (2)$$

where r_d and z_d are the radial and vertical distances, respectively. $n_{d,0} = \rho_{d,0}/\mu m_p$ is the disc base number density at R_\star , where $\mu \sim 0.62$ is the molecular weight in the disc and the density of the disk near stellar surface $\rho_{d,0}$ is between $10^{-13} \text{ g cm}^{-3}$ and $10^{-10} \text{ g cm}^{-3}$ (Rivinius et al. 2013). $\beta_d = 2 - 4$ is the disc density

slope (Rivinius et al. 2013). The scale height of the disc is

$$H(r_d) = c_s \left(\frac{r_d}{GM_\star} \right)^{1/2} r_d, \quad (3)$$

where M_\star is the star mass and $c_s = (kT_\star/\mu m_p)^{1/2}$ is the isothermal sound speed.

The orbital angular momentum is in the z -direction and the magnetic axis inclination angle is i_m (see Fig. 2). The magnetic field of the star is dipole ($B \propto r^{-3}$) within the Alfvén radius R_A . The magnetic field will become radial at a large distance because of the drag effect of the stellar wind and the fast rotation of OB stars will make the magnetic field become toroidal (Usov & Melrose 1992). Thus, for a massive star, the magnetic field in the stellar wind or disc can be described as (Melatos et al. 1995; Yang et al. 2022b)

$$B_s(r) \sim \begin{cases} B_0 \left(\frac{r}{R_\star} \right)^{-3}, & R_\star < r < R_A, \\ B_0 \left(\frac{R_A}{R_\star} \right)^{-3} \left(\frac{r}{R_A} \right)^{-\alpha}, & r > R_A, \end{cases} \quad (4)$$

where B_0 is the magnetic field strength at R_\star . We have $\alpha = 2$ for a radial field and $\alpha = 1$ for a toroidal field. The Alfvén radius R_A can be estimated by the balance of the stellar wind's ram pressure and the magnetic pressure

$$\frac{1}{2} \rho_w (R_A) v_w^2 \simeq \frac{1}{8\pi} B(R_A)^2. \quad (5)$$

The RM variations of HMGBs (e.g., PSR B1259–63/LS 2883 Johnston et al. 1996) can be well understood in the context of toroidal field in stellar disc (Melatos et al. 1995). The temperature of the stellar wind decay with the following power-law because of adiabatic cooling (Kochanek 1993; Bogomazov 2005)

$$T_w(r) = T_\star \left(\frac{r}{R_\star} \right)^{-\beta_w}, \quad (6)$$

where T_\star is the surface effective temperature of the star and $\beta_w = 2/3$. The temperature profile of the vertically isothermal disc is given by (Carciofi & Bjorkman 2006)

$$T_d(r_d) = \frac{T_\star}{\pi^{1/4}} \left[\arcsin \left(\frac{R_\star}{r_d} \right) - \left(\frac{R_\star}{r_d} \right) \sqrt{1 - \left(\frac{R_\star}{r_d} \right)^2} \right]^{1/4}. \quad (7)$$

The parameters of the massive star we adopted are: the stellar mass $M_\star = 30 M_\odot$, the stellar radius $R_\star = 10 R_\odot$, the surface effective temperature $T_\star = 2 \times 10^4$ K and the wind velocity $v_w = 3 \times 10^8$ cm s⁻¹, which are consistent with the observations (e.g., LS 2883 Negueruela et al. 2011; LS 5039 Casares et al. 2005).

2.2. The terminal shock

The pulsar wind will be terminated by the stellar wind and the wind interactions will form a bow shock cavity, which is shown in Fig. 1(b). The momentum rate ratio of the pulsar and the stellar wind is defined as

$$\eta = \frac{L_{sd}/c}{\dot{M} v_w}, \quad (8)$$

where L_{sd} is the spin-down luminosity of the pulsar. If $\eta > 1$, the pulsar wind is stronger, and the shock bend back to the star. In this case, there is no RM variation for most orbital phase, which contradicts with

the observations of repeating FRBs. Therefore, we consider the case of $\eta < 1$. The distances from the termination shock to the pulsar and massive star are

$$r_s = d \frac{\eta^{1/2}}{1 + \eta^{1/2}}, \quad (9)$$

and

$$R_s = d \frac{1}{1 + \eta^{1/2}}, \quad (10)$$

respectively. The orbital separation d at phase ϕ is

$$d = \frac{a(1 - e^2)}{1 + e \cos \phi}, \quad (11)$$

where e is the eccentricity of the orbit. The semimajor axis a is given by Kepler's third law

$$\frac{P_{\text{orb}}^2}{a^3} = \frac{4\pi^2}{G(M_\star + m)}, \quad (12)$$

where P_{orb} is the orbital period, M_\star and $m = 1.4 M_\odot$ are the mass of massive star and pulsar, respectively.

To calculate the DM, RM and the free-free optical depth along the LOS, we adopt the geometric description of the binary system from [Chen et al. \(2021\)](#). As shown in Fig. 1(a), the unit vector of the observer is

$$\mathbf{e}_{\text{obs}} = (\sin i_o \cos \phi_o, \sin i_o \sin \phi_o, \cos i_o), \quad (13)$$

where i_o and ϕ_o are the inclination angle and true anomaly of the observer, respectively. The normal unit vector of the disc is

$$\mathbf{e}_{\text{disc}} = (\sin i_d \cos \phi_d, \sin i_d \sin \phi_d, \cos i_d), \quad (14)$$

where i_d and ϕ_d are the inclination angle and true anomaly of the disc normal unit vector, respectively. As shown in Fig. 1(b), the unit vector in the direction connecting any point along the LOS to the massive star is

$$\mathbf{e}_r = (d \cdot \mathbf{e}_{\text{psr}} + l \cdot \mathbf{e}_{\text{obs}}) / r, \quad (15)$$

where $\mathbf{e}_{\text{psr}} = (\cos \phi, \sin \phi, 0)$ is the unit vector in the direction of the pulsar and l is the distance from the pulsar. The distance from the arbitrary point along LOS to the massive star is

$$r^2 = d^2 + l^2 + 2dl(\mathbf{e}_{\text{psr}} \cdot \mathbf{e}_{\text{obs}}). \quad (16)$$

If the LOS passes through the stellar disc, the radial and vertical distances in the disc are given by

$$r_d = r \sin \theta, z_d = r \cos \theta, \quad (17)$$

where $\theta = \arccos(\mathbf{e}_r \cdot \mathbf{e}_{\text{disc}})$ is the angle between the arbitrary radial direction from the star and the disc normal direction.

3. DM AND RM VARIATIONS

The observed DM and RM of a cosmological-origin FRB (with the redshift z) are contributed by different parts, including the local environment of FRBs, the host galaxy, the intergalactic medium (IGM) and the Milky Way (MW):

$$\text{DM}_{\text{obs}} = \text{DM}_{\text{MW}} + \text{DM}_{\text{IGM}} + \frac{\text{DM}_{\text{host}} + \text{DM}_{\text{source}}}{1 + z}, \quad (18)$$

$$\text{RM}_{\text{obs}} = \text{RM}_{\text{MW}} + \text{RM}_{\text{IGM}} + \frac{\text{RM}_{\text{host}} + \text{RM}_{\text{source}}}{(1 + z)^2}. \quad (19)$$

Along the paths of FRBs, the medium in MW, IGM and host galaxies are stable on a relatively short time scale. Therefore, the DM and RM variations mainly come from the local plasma of sources, including the contributions from the pulsar wind, the terminal shock shell and the stellar outflows. The electron number density in the pulsar wind can be negligible compared to the stellar wind of massive stars ($n_{\text{BE}} \sim 10^7 n_{\text{PS}}$, see [Melatos et al. 1995](#)). What's more, the DM and RM from relativistic electrons should be reduced by a factor of γ^2 , with γ being the Lorentz factor of electrons ([Quataert & Gruzinov 2000](#)). Thus, the RM contributed by a pulsar wind is very small and can be ignored.

The thickness h of the terminal shocked shell at the apex is $h = \frac{1}{8} \min(r_s, R_s)$ ([Luo et al. 1990](#)). The shocked material will lose its energies via adiabatic or radiative cooling processes. The adiabatic dominated shock radiation is consistent with the photon index of keV X-ray and TeV γ -ray spectrum from PSR B1259–63/LS 2883 ([Chen et al. 2019](#)). In this case, the asymptotic opening angle between the reverse shock and the contact surface is $\Delta\psi \sim 0$ ([Luo et al. 1990](#)). Different from the extended SNR shock shell ([Yang & Zhang 2017](#); [Piro & Gaensler 2018](#); [Zhao et al. 2021](#); [Zhao & Wang 2021](#)), the DM and RM from the terminal shock shell are also unimportant.

The DM and RM variations from the stellar wind or disc are

$$\begin{aligned} \Delta\text{DM} &= \int_{\text{LOS}} n_e dl, \\ \Delta\text{RM} &= 8.1 \times 10^5 \int_{\text{LOS}} n_e \mathbf{B} \cdot d\mathbf{l}, \end{aligned} \quad (20)$$

where the electron number density n_e (in units of cm^{-3}), the magnetic field \mathbf{B} (in units of G) and the distance l (in units of pc) are given in Section 2. The free-free absorption coefficient is ([Rybicki & Lightman 1979](#))

$$\alpha_{\nu}^{\text{ff}} = 0.018 T^{-3/2} z_i^2 n_e n_i \nu^{-2} \bar{g}_{\text{ff}}, \quad (21)$$

where the Gaunt factor $\bar{g}_{\text{ff}} \sim 1$ and the atomic number of the ion $z_i \sim 1$ are used in this work. The free-free optical depth of the stellar outflow is

$$\tau(\nu) = \int_{\text{LOS}} \alpha(\nu) dl. \quad (22)$$

Because we neglect the contributions from the pulsar wind and the terminal shock shell, we can get the DM, RM and $\tau(\nu)$ integrating from the joining point of the LOS and the shock contact discontinuity (CD) surface to infinity numerically. As shown in Fig. 1(b), points S, P and Q are the intersection points of LOS and the shock CD surface, arbitrary radial direction of stellar wind and disc, respectively. The pulsar and massive star are regarded as mass points, denoted as points M and O, respectively. The distance from the bow shock CD surface to the pulsar is ([Cantó et al. 1996](#))

$$l_s = d \sin \theta_s \csc(\theta_s + \theta_p), \quad (23)$$

where θ_s and θ_p are the angles between the line connecting the two stars and the line SM and SO, respectively. For most HMXBs, the pulsar wind is much weaker than that of stars ($\eta \ll 1$). In this way, the angle θ_s is approximated as follows (Cantó et al. 1996)

$$\theta_s = \left\{ \frac{15}{2} \left[\sqrt{1 + \frac{4}{5}\eta(1 - \theta_p \cot \theta_p)} - 1 \right] \right\}^{1/2}, \quad (24)$$

where

$$\theta_p = \pi - \arccos(\mathbf{e}_{\text{psr}} \cdot \mathbf{e}_{\text{obs}}) \quad (25)$$

depends on the orbital phase.

3.1. DM and RM from the stellar wind: application to FRB 20180916B

A periodic (~ 16.35 d) bursting activity was found for FRB 20180916B (CHIME/FRB Collaboration et al. 2020b), which may originate from orbital motion (Dai & Zhong 2020; Ioka & Zhang 2020; Lyutikov et al. 2020; Gu et al. 2020; Li et al. 2021b; Wada et al. 2021), precession (Levin et al. 2020; Tong et al. 2020; Yang & Zou 2020; Zanazzi & Lai 2020; Katz 2021b; Sridhar et al. 2021; Li & Zanazzi 2021; Wei et al. 2022; Chen et al. 2022) or ultralong spin of magnetars (Beniamini et al. 2020). The chromaticity was first found by Pleunis et al. (2021) and Pastor-Marazuela et al. (2021). Very recently, Bethapudi et al. (2022) extended the chromatic activity window of FRB 20180916B to higher frequencies. The chromaticity is consistent with binary models described in Wada et al. (2021) or slowly rotating/freely precessing models described in Li & Zanazzi (2021). However, the RM variations are unrelated to the ~ 16.35 d period (Mckinven et al. 2022), which is inconsistent with the quasi-periodic variations of a binary system. Thus, the assumption of the 16.35-day period being from a precessing (or rotating) magnetar is used in this work. The burst is produced by the coherent curvature radiation in the magnetar’s magnetosphere (Yang & Zhang 2018; Lu et al. 2020) and the chromaticity is caused by the altitude-dependent radio emission (Li & Zanazzi 2021). In addition, the clustered polarization position angles (PPAs) in phase have been found (Bethapudi et al. 2022), which has been predicted in Li & Zanazzi (2021).

Motivated by the observations that the RM variation is unrelated to the 16.35-day period (Mckinven et al. 2022), we consider that FRB 20180916B is in a binary with a long orbital period (see Fig. 1). The secular RM variation may be caused by the periastron or superior conjunction (SUPC) passage of the pulsar in an HMXB or an HMGB. In this way, the current observations of FRB 20180916B can be explained simultaneously.

Below, we fit the RM variation of FRB 20180916B. The typical values we adopted are listed in Table 1. To explain nearly non-evolved RM from the year 2018 to 2021 and the secular decrease of $|\text{RM}|$ from 2021 April to 2021 December (Mckinven et al. 2022), the orbital period must be longer than 3 yr. It must be noted that this orbital period is not related to the orbiting models producing the periodic activity of this source. The fitting results for the cases of $P = 1600$ d, $e = 0.5$ (Model A) and $P = 2000$ d, $e = 0.5$ (Model B) are shown in Fig. 3 and the parameters are listed in Table 2. For the case of the stellar wind, the magnetic axis inclination angle is assumed to be $\sim 0^\circ$ and the discussion of different magnetic axis inclination angles is given in Section 5.1.2. The blue circles represent the observed RM variations $\Delta\text{RM}_{\text{obs}} = \text{RM}_{\text{obs}} - \text{RM}_{\text{obs},0}$ from Mckinven et al. (2022), and $\text{RM}_{\text{obs},0} = -114 \text{ rad m}^{-2}$ is the value of the nearly non-evolving phase (CHIME/FRB Collaboration et al. 2020b; Nimmo et al. 2021; Pastor-Marazuela et al. 2021; Mckinven et al. 2022). RM variations are shown in red curves, defined as $\Delta\text{RM} = \text{RM}(t) - \text{RM}_0$, where RM_0 is the minimum value of the orbital modulated RM occurring around apastron or inferior conjunction (INFC).

For Model A, the magnetic field of stellar wind is assumed to be radial ($\mathbf{B}_s = B_0 (R_A/R_\star)^{-3} (r/R_A)^{-2} \mathbf{e}_r$). The spin-down luminosity is $L_{\text{sd}} = 10^{36} \text{ erg s}^{-1}$, which is consistent with the observations of the pulsars in Be/X-ray binaries (e.g., $L_{\text{sd}} = 8 \times 10^{35} \text{ erg s}^{-1}$ for PSR B1259–63 [Manchester et al. 1995](#)). The mass-loss rate and the stellar surface magnetic field is $10^{-8} M_\odot \text{ yr}^{-1}$ and 5 G, respectively. The periastron time T_0 is on MJD 59650. Near periastron, RM variations reach the peak. For radial magnetic field in the wind, RM will not change sign before and after periastron. The toroidal magnetic field ($\mathbf{B}_s = B_0 (R_A/R_\star)^{-3} (r/R_A)^{-1} \mathbf{e}_\phi$) in the stellar wind is used in Model B. The spin-down luminosity is $L_{\text{sd}} = 2 \times 10^{35} \text{ erg s}^{-1}$, which is similar as that of PSR J2032+4127 ([Camilo et al. 2009](#)). The mass-loss rate, the stellar surface magnetic field and the periastron time are $10^{-9} M_\odot \text{ yr}^{-1}$, 2 G and MJD 59900, respectively. For the case of the toroidal magnetic field, RM will reverse before and after the SUPC ($T_{\text{SUPC}} = -83.4 \text{ d}$).

The radio signals from HMXBs with short periods will be obscured due to the free-free absorption of stellar outflows, such as LS I +61°303 (see the study of [Zdziarski et al. 2010](#)). Nonetheless, we can still receive the radio signals when the pulsar wind cavity¹ points toward us, which has been proposed to explain the ‘active window’ of periodic FRBs ([Ioka & Zhang 2020](#); [Lytikov et al. 2020](#); [Wada et al. 2021](#)). However, the RM variations are unrelated to the 16.35-day period ([Mckinven et al. 2022](#)). Here, we consider that the RM variations are caused by the long orbital period. The DM contributions and the free-free optical depth of the stellar wind are shown in Fig. 4. The DM variations and the free-free absorption process can be neglected, which is consistent with observations ([Chawla et al. 2020](#); [CHIME/FRB Collaboration et al. 2020b](#); [Nimmo et al. 2021](#); [Pastor-Marazuela et al. 2021](#); [Pleunis et al. 2021](#); [Mckinven et al. 2022](#)).

3.2. DM and RM from the stellar disc: application to FRB 20180916B

Some massive stars, i.e., Be stars, have a decretion disk, which is considered the origin of the emission lines and infrared excess ([Reig 2011](#); [Rivinius et al. 2013](#)). The orbital plane and the disc are usually misaligned in a Be/X-ray binary due to supernova kicks of pulsars ([Brandt & Podsiadlowski 1995](#); [Martin et al. 2009](#)). However, the disc inclination angle is still unknown. From the observations, the disc inclination angle is found to be from 25° to 70° for PSR B1259–63/LS 2883 ([Martin et al. 2009](#)). By fitting to the DM and RM variations of PSR B1259–63, the disc inclination angle is found to be from 10° to 40° ([Melatos et al. 1995](#)). However, a large inclination angle $i_d = 45^\circ$, $i_d = 60^\circ$ or $i_d = 70^\circ$ is also possible given by the study of radio absorption ([Chen et al. 2021](#)), multi-wavelength emissions ([Chen et al. 2019](#)) or XMM–Newton observations ([Chernyakova et al. 2006](#)) from PSR B1259–63/LS 2883. In this work, the disc inclination angle $i_d = 60^\circ$ is used. The magnetic axis direction is assumed the same as that of the disc normal vector. The disc will be truncated due to the tidal torques from the pulsar ([Reig 2011](#)), especially in circular orbits ([Okazaki et al. 2011](#)). Here, we will discuss the case of the Be/X-ray binaries with high orbital eccentricity to avoid disc truncation. The true anomaly angle of the inclined equatorial disc projected on the orbital plane is ([Chen et al. 2019, 2021](#))

$$\Delta\phi_d = \sin^{-1} \left(\frac{\sin \Delta\theta_d}{\sin i_d} \right), \quad (26)$$

where $\Delta\theta$ is the half-opening angle of the disc. The pulsar will pass through the inclined disc twice before and after periastron ($\phi \in [\phi_d - \pi/2 - \Delta\phi_d, \phi_d - \pi/2 + \Delta\phi_d]$ and $\phi \in [\phi_d + \pi/2 - \Delta\phi_d, \phi_d + \pi/2 + \Delta\phi_d]$). When the pulsar passes through the disc, the pressure from the disc will further push the shock surface

¹ For the short-period system, the pulsar wind cavity will become a spiral-shape (or a funnel-shape used in [Ioka & Zhang 2020](#)) due to the strong Coriolis shock ([Bosch-Ramon & Barkov 2011](#); [Bosch-Ramon et al. 2015](#)). However, the effect caused by Coriolis force can be ignored for the long-period system ([Chen et al. 2021](#)).

towards the pulsar and make the momentum rate ratio η reduced. From the estimation of [Chen et al. \(2019\)](#), the additional pressure from the disc makes $\sim 0.01\eta$.

The fitting result of RM variations from the stellar wind and disc (Model C) is shown in panel (c) of Fig. 3. The spin-down luminosity is $L_{\text{sd}} = 10^{36}$ erg s $^{-1}$. The disc density slope $\beta_d = 3.5$ is used ([Carciofi & Bjorkman 2006](#); [Rivinius et al. 2013](#)). The parameters of the stellar wind and disc models are listed in Table 2. The period and the orbital eccentricity of the binary system are $P = 16000$ d and $e = 0.86$, respectively. The orbital parameters are similar to the Be/X-ray binary PSR J2032+4127/MT91 213 ($P = 16000 - 17000$ d, $e \sim 0.9$) estimated by [Ho et al. \(2017\)](#). Follow the study of RM variations of PSR B1259–63, the toroidal magnetic field ($\mathbf{B}_s = B_0 (R_A/R_\star)^{-3} (r/R_A)^{-1} \mathbf{e}_\phi$) in the disc is used and the magnetic field in the stellar wind is assumed to be radial ($\mathbf{B}_s = B_0 (R_A/R_\star)^{-3} (r/R_A)^{-2} \mathbf{e}_r$) ([Melatos et al. 1995](#)). The mass-loss rate and the stellar surface magnetic field is $10^{-8} M_\odot \text{ yr}^{-1}$ and 1 G, respectively. The half-opening angle of the disc is $\Delta\theta = 15^\circ$ ([Waters 1986](#)). In this case, the RM is dominated by the disc. The periastron time is on MJD 59700. The pulsar will pass through the inclined disc twice before and after periastron. The orange-shaded regions represent the time when the pulsar passes through the disc. The pressure from the disc will reduce the momentum rate ratio of the pulsar and the stellar wind ($\sim 0.01\eta$). For Model C, the disc direction is set as $(i_d, \phi_d) = (60^\circ, 180^\circ)$. The disc direction will significantly affect the RM profiles (see Section 5.1.3). The radio signals travel through different components of the disc when a pulsar passes through the disc near periastron, which leads to complicated RM variations (e.g., with some minor structures and multiple reversals).

The DM contributions and the free-free optical depth of Model C (see Fig. 4) are also unimportant. Both DM and the free-free optical depth from the disc show the asymmetric profile before and after the periastron.

4. CLUMPS IN STELLAR WIND AND DISC

The density of the smooth stellar wind and disc is discussed in Section 3. However, the stellar wind ([Moffat & Robert 1994](#); [Puls et al. 2006](#)) or disc ([Chernyakova et al. 2021](#)) are found to be clumpy from observations. The size of the inhomogeneities is estimated to be $\sim 10^{10} - 10^{11}$ cm from the several hours-duration X-ray flares of the Be star binary system 2S 0114+65 ([Apparao et al. 1991](#)). The short variability on GeV light curve (between a few minutes to a few days) is also found from the 2017 ([Chernyakova et al. 2020](#)) and 2021 periastron passage ([Chernyakova et al. 2021](#)) of PSR B1259–63/LS 2883. The GeV flares are thought to be caused by the bremsstrahlung emission from the clumps in the stellar wind ([Chernyakova et al. 2020](#)). The typical size of the clumps can be estimated as

$$l_c \sim v \Delta t_f = 7.2 \times 10^{10} \text{ cm} \left(\frac{M_{\text{tot}}}{30 M_\odot} \right)^{1/2} \left(\frac{a}{1 \times 10^{13} \text{ cm}} \right)^{-1/2} \left(\frac{\Delta t_f}{1 \text{ h}} \right), \quad (27)$$

where v is the Keplerian velocity of the pulsar and Δt_f is the durations of the flares. The clumps enhance the density by a factor of $1/f$ compared to the smooth stellar outflows, with f being the filling factor. From observations, the filling factor of the stellar wind is $f \sim 0.1$ ([Moffat & Robert 1994](#); [Puls et al. 2006](#)). The inhomogeneities of the density and magnetic field in clumps would lead to stochastic DM and RM variations, which have been detected ([Pleunis et al. 2021](#); [Mckinven et al. 2022](#)). The minor structures of RM evolution of FRB 20201124A are considered to be caused by the clumps in the disc ([Wang et al. 2022a](#)). We will give the DM and RM contributions only from the density inhomogeneities of clumps ([Melatos et al. 1995](#)).

From our estimation in Section 3 ($P = 1600 - 16000$ d, $M_{\text{tot}} \sim 30 M_\odot$), the distance from the massive star around periastron is $d \sim 10^{14}$ cm. As shown in Fig. 5, clumpy stellar wind/disc interacts with the pulsar

wind and X-ray/GeV γ -ray flares generate when clumps enter the LOS. The clump density in stellar wind is $n_{c,w} = n_w(D)/f$, where D is the distance between clumps and the massive star. For simplicity, we assume the disc clumps are on the mid-plane of the disc. Thus, the clump density in stellar disc is $n_{c,d} = n_d(D)/f$. The DM from the clumps in stellar wind and disc is

$$\text{DM}_{c,w} \sim 0.0016 \text{ pc cm}^{-3} \left(\frac{n_{w,0}}{10^8 \text{ cm}^{-3}} \right) \left(\frac{D}{10^{14} \text{ cm}} \right)^{-2} \left(\frac{f}{0.1} \right)^{-1} \left(\frac{l_c}{10^{11} \text{ cm}} \right), \quad (28)$$

$$\text{DM}_{c,d} \sim 0.001 \text{ pc cm}^{-3} \left(\frac{n_{d,0}}{10^{11} \text{ cm}^{-3}} \right) \left(\frac{D}{10^{14} \text{ cm}} \right)^{-3.5} \left(\frac{f}{0.1} \right)^{-1} \left(\frac{l_c}{10^{11} \text{ cm}} \right). \quad (29)$$

The RM from the radial magnetic field in the stellar wind is

$$\text{RM}_{c,w} \sim 0.06 \text{ rad m}^{-2} \left(\frac{n_{d,0}}{10^{11} \text{ cm}^{-3}} \right) \left(\frac{B_0}{1 \text{ G}} \right) \left(\frac{D}{10^{14} \text{ cm}} \right)^{-4} \left(\frac{f}{0.1} \right)^{-1} \left(\frac{l_c}{10^{11} \text{ cm}} \right). \quad (30)$$

For a toroidal magnetic field, the RM from the clumpy wind is

$$\text{RM}_{c,w} \sim 8.8 \text{ rad m}^{-2} \left(\frac{n_{w,0}}{10^8 \text{ cm}^{-3}} \right) \left(\frac{B_0}{1 \text{ G}} \right) \left(\frac{D}{10^{14} \text{ cm}} \right)^{-3} \left(\frac{f}{0.1} \right)^{-1} \left(\frac{l_c}{10^{11} \text{ cm}} \right). \quad (31)$$

The RM from the clumps on the mid-plane of the disc is

$$\text{RM}_{c,d} \sim 5.1 \text{ rad m}^{-2} \left(\frac{n_{d,0}}{10^{11} \text{ cm}^{-3}} \right) \left(\frac{B_0}{1 \text{ G}} \right) \left(\frac{D}{10^{14} \text{ cm}} \right)^{-4.5} \left(\frac{f}{0.1} \right)^{-1} \left(\frac{l_c}{10^{11} \text{ cm}} \right). \quad (32)$$

The nearly unchanged DM and small RM fluctuations are consistent with the observations (Pleunis et al. 2021; Mckinven et al. 2022). The discussions above are based on the assumption that the inhomogeneities only affect clumps' density. However, the magnetic field in clumps will also contribute to the RM variations although the magnetic field in clumps is still unknown. The sudden RM reversal in a few days through the 2004 periastron passage of PSR B1259–63 (Johnston et al. 2005) favors a scenario in which the magnetic field reverses in clumps. Whether the RM reversal can be observed on short timescales (i.e., < 1 day) remains to be tested for FRBs.

5. DISCUSSION

5.1. DM and RM variations for other repeating FRBs or massive binaries

5.1.1. DM and RM variations in FRB 20121102A

DM and RM variations were first detected in FRB 20121102A. The increasing DM (Hessels et al. 2019; Josephy et al. 2019; Oostrum et al. 2020; Li et al. 2021a) and decreasing RM (Michilli et al. 2018; Hilmarsson et al. 2021) was found from long-term observations. The DM and RM variations may be from the wind nebula and the ejecta of a young magnetar born in the merger of a compact binary (Zhao et al. 2021). A possible period of ~ 160 d was reported for FRB 20121102A (Rajwade et al. 2020; Cruces et al. 2021). Due to lack the study of chromaticity, the origin of periodicity is difficult to determine. Interestingly, its DM has been found to be $552.5 \pm 0.9 \text{ pc cm}^{-3}$ from the recent observations (Wang et al. 2022b), which has decreased by $\sim 10 \text{ pc cm}^{-3}$ from that of Li et al. (2021a). If the decrease of DM can be further confirmed by subsequent observations, the DM variations can be well-understood in our model. Due to the difference in

pulsar wind cavity size along the LOS at different orbital phases, the evolution of the DM before and after periastron can be asymmetric (see Fig. 4).

The extreme RM ($\sim 10^5$ rad m^{-2} , Michilli et al. 2018; Hilmarsson et al. 2021) of FRB 20121102A may be from the compact PRSs (Margalit & Metzger 2018; Zhao & Wang 2021; Yang et al. 2022a; Sridhar & Metzger 2022). Therefore, there may be two possible RM evolution trends of FRB 20121102A afterward. If the RM from the binary (RM_b , e.g., from the stellar wind/disc or clumps) is much smaller than that from PRS, RM will just decrease. However, if $RM_b \simeq RM_{PRS}$, the irregular RM variations or reversals will be detected.

5.1.2. RM variations and reversals in FRB 20190520B

The RM variations and reversals of FRB 20190520B (Anna-Thomas et al. 2022; Dai et al. 2022) have been discussed in Wang et al. (2022a) and Dai et al. (2022) using the binary model. Dai et al. (2022) consider that the FRB source orbits around a magnetized companion (e.g., a massive black hole or a massive star). The large-scale magnetic field is radial. The pulsar will travel through the magnetic field reversal region when the pulsar orbit is edge-on with respect to the magnetic axis. Here, we will give a general description of the case of the radial magnetic field. The orbital-dependent normalized RM variations of different magnetic axis inclination angles are shown in Fig. 6(a), and other parameters are the same as Model A. We can see that the RM does not reverse, except if the magnetic axis inclination angle is close to 90° .

Another explanation introduces the toroidal magnetic field in the decretion disc of a Be star (Wang et al. 2022a). In this work, some complex RM variations caused by the additional pressure and the clumps from the disc are also considered, which can be checked by future observations. In addition to the above two cases, the toroidal magnetic field in the stellar wind is also possible.

5.1.3. Complicated RM variations in FRB 20201124A and PSR B1259–63

The irregular RM variations and multiple reversals in one cycle have been observed for FRB 20201124A (Xu et al. 2022) and PSR B1259–63 (Johnston et al. 1996; Connors et al. 2002; Johnston et al. 2005). For PSR B1259–63, RMs can even be different between two periastron passages (Johnston et al. 1996; Connors et al. 2002; Johnston et al. 2005). The complexity of RM variations may not be explained by uncertainties in orbital parameters and observation angles because these parameters are well constrained by pulsar timing and very long baseline interferometric observations (Shannon et al. 2014; Miller-Jones et al. 2018). There are several possible reasons for the complexity of RM variations. First, some random variations or even reversals are caused by the clumps in the stellar wind/disc (Wang et al. 2022a). Second, RM contributed by the stellar wind and disc (or/and the radial and toroidal magnetic field) both exist, which results in a multimodal and multiple reversal profile of the RM evolution. Third, the disc direction will have a great impact on the evolution of RM. The complicated RM profiles of different disc directions are shown in Fig. 6(b), and other parameters are the same as Model C. Fourth, the local disc density and magnetic field may be different when the pulsar enters the disc (Johnston et al. 2005), which may be the reason why RMs are different between two periastron passages (Johnston et al. 1996; Connors et al. 2002; Johnston et al. 2005).

The complicated RM variations caused by the disc can be distinguished by their behavior near periastron (see Fig. 6(b)). For PSR B1259–63, the pulsar is eclipsed by the dense stellar outflows around periastron. Luckily, the eclipsing seems to be not important for FRB 20201124A (Xu et al. 2022; Wang et al. 2022a). The interaction between the pulsar and the disc makes RM_{disc} unpredictable. However, from the observations of different periastron passages of PSR B1259–63 (Johnston et al. 1996; Connors et al. 2002; Johnston et al. 2005), the evolutionary trend of the RM is similar after the pulsar leaves the disc. Different

from the disc, stellar winds are stable on long-time scales. The eclipse near periastron is mainly caused by the stellar wind for PSR B1259–63, which will not be significantly different during different periastron passages. Thus, constraints on orbital parameters and complex environments can still be given via the long-term monitoring of FRB 20201124A.

5.2. Compact persistent radio sources

FRB 20121102A (Chatterjee et al. 2017) and FRB 20190520B (Niu et al. 2022) are associated with compact luminous ($\nu L_\nu \sim 10^{39}$ erg s⁻¹) PRSs. The compact PRS may be from a magnetar wind nebula (Margalit & Metzger 2018; Zhao & Wang 2021), a magnetized plasma screen (Yang et al. 2022a) or ultraluminous X-ray hypernebulae (Sridhar & Metzger 2022). All the above models consider PRSs to be associated with large RMs ($\sim 10^4 - 10^5$ rad m⁻²) and that the age of center engine is very young (e.g., 14-22 yr in Zhao & Wang 2021 and 10 yr in Sridhar & Metzger 2022). There is no evidence for the PRS of FRB 20180916B (Marcote et al. 2020).

Considering that the binary model of Sridhar & Metzger (2022) has evolved as a common-envelope precursor, we will not discuss this model here. Besides, there are two possible origins of luminous PRS in massive binaries: the scaled-down pulsar wind nebulae (PWNe, Margalit & Metzger 2018; Zhao & Wang 2021) in HMGBs or the companion wind as the plasma screen (Yang et al. 2022a). The structures of the compact scaled-down PWNe have been found in HMGBs (Neronov & Chernyakova 2007; Zdziarski et al. 2010). As discussed in Zhao & Wang (2021), the interior magnetic energy of young magnetars will be injected into the surroundings (here being the scaled-down PWNe or the companion wind) via energetic magnetar flares and synchrotron radiation of relativistic electrons produce luminous PRSs.

6. SUMMARY

Recently, the RM variations or even reversals have been observed for FRB 20121102A (Michilli et al. 2018), FRB 20201124A (Xu et al. 2022), FRB 20190520B (Anna-Thomas et al. 2022; Dai et al. 2022) and FRB 20180916B (Pleunis et al. 2021; Mckinven et al. 2022), which are similar to the RM changes of PSR B1259–63/LS 2883. Some binary models have been proposed to explain the RM variations and reversals (Dai et al. 2022; Wang et al. 2022a). Compared to previous work, we give a more general description of the DM, RM and free-free absorption process from a massive binary system. We study the contributions of RM, DM and free-free absorption process from the stellar wind and disc, and fit the RM variations of FRB 20180916B. This paper presents the effects of orbital geometry, magnetic field structure, the pulsar wind cavity, observation (magnetic axis, disc) orientation and the clumpy stellar wind/disc on DM/RM variations, and these differences can be tested by subsequent observations. Our conclusions are summarized as follows.

- For the case of the radial magnetic field in the stellar wind, RM will not reverse except if the magnetic axis inclination angle is close to 90°. However, for the toroidal magnetic field in the stellar wind, RM will reverse before and after the SUPC.
- For the case of the toroidal disc magnetic field domain, the RM variations become complicated when the pulsar passes through the inclined disc twice, i.e., before and after periastron. The RM from the disc may have a multimodal and multiple reversal profile because the radio signals travel through different components of the disc during periastron passage. What's more, the interaction between the pulsar and the disc makes RM different between two periastron passages (Johnston et al. 1996; Connors et al. 2002; Johnston et al. 2005).

- In this work, we assume the 16.35-day period and the chromaticity are from a slowly rotating or freely precessing magnetar (Li & Zanazzi 2021). The secular RM variations of FRB 20180916B are raised from periastron passage of a pulsar with the orbital period of $\sim 1600 - 16000$ d. The DM and free-free absorption contributed by the stellar wind and disc are negligible.
- When the clumps in stellar wind or disc interact with FRBs, the inhomogeneities of the density and magnetic field in clumps would lead to stochastic RM variations or even reversals.

ACKNOWLEDGEMENTS

We thank the anonymous referee for helpful comments, and Yuan-Pei Yang and A-Ming Chen for helpful discussions. This work was supported by the National Natural Science Foundation of China (grant Nos. 12273009, U1831207 and 11833003), the National Key Research and Development Program of China (grant No. 2017YFA0402600), the National SKA Program of China (grant Nos. 2020SKA0120300 and 2022SKA0130100), and the China Manned Space Project (CMS-CSST-2021-A12).

REFERENCES

- Anna-Thomas, R., Connor, L., Burke-Spolaor, S., et al. 2022, arXiv e-prints, arXiv:2202.11112. <https://arxiv.org/abs/2202.11112>
- Apparao, K. M. V., Bisht, P., & Singh, K. P. 1991, ApJ, 371, 772, doi: [10.1086/169941](https://doi.org/10.1086/169941)
- Beloborodov, A. M. 2017, ApJL, 843, L26, doi: [10.3847/2041-8213/aa78f3](https://doi.org/10.3847/2041-8213/aa78f3)
- Beniamini, P., Wadiasingh, Z., & Metzger, B. D. 2020, MNRAS, 496, 3390, doi: [10.1093/mnras/staa1783](https://doi.org/10.1093/mnras/staa1783)
- Bethapudi, S., Spitler, L. G., Main, R. A., Li, D. Z., & Wharton, R. S. 2022, arXiv e-prints, arXiv:2207.13669. <https://arxiv.org/abs/2207.13669>
- Bochenek, C. D., Ravi, V., Belov, K. V., et al. 2020, Nature, 587, 59, doi: [10.1038/s41586-020-2872-x](https://doi.org/10.1038/s41586-020-2872-x)
- Bogomazov, A. I. 2005, Astronomy Reports, 49, 709, doi: [10.1134/1.2045321](https://doi.org/10.1134/1.2045321)
- Bosch-Ramon, V., & Barkov, M. V. 2011, A&A, 535, A20, doi: [10.1051/0004-6361/201117235](https://doi.org/10.1051/0004-6361/201117235)
- Bosch-Ramon, V., Barkov, M. V., & Perucho, M. 2015, A&A, 577, A89, doi: [10.1051/0004-6361/201425228](https://doi.org/10.1051/0004-6361/201425228)
- Brandt, N., & Podsiadlowski, P. 1995, MNRAS, 274, 461, doi: [10.1093/mnras/274.2.461](https://doi.org/10.1093/mnras/274.2.461)
- Camilo, F., Ray, P. S., Ransom, S. M., et al. 2009, ApJ, 705, 1, doi: [10.1088/0004-637X/705/1/1](https://doi.org/10.1088/0004-637X/705/1/1)
- Cantó, J., Raga, A. C., & Wilkin, F. P. 1996, ApJ, 469, 729, doi: [10.1086/177820](https://doi.org/10.1086/177820)
- Carciofi, A. C., & Bjorkman, J. E. 2006, ApJ, 639, 1081, doi: [10.1086/499483](https://doi.org/10.1086/499483)
- Casares, J., Ribó, M., Ribas, I., et al. 2005, MNRAS, 364, 899, doi: [10.1111/j.1365-2966.2005.09617.x](https://doi.org/10.1111/j.1365-2966.2005.09617.x)
- Chatterjee, S., Law, C. J., Wharton, R. S., et al. 2017, Nature, 541, 58, doi: [10.1038/nature20797](https://doi.org/10.1038/nature20797)
- Chawla, P., Andersen, B. C., Bhardwaj, M., et al. 2020, ApJL, 896, L41, doi: [10.3847/2041-8213/ab96bf](https://doi.org/10.3847/2041-8213/ab96bf)
- Chen, A. M., Guo, Y. D., Yu, Y. W., & Takata, J. 2021, A&A, 652, A39, doi: [10.1051/0004-6361/202140951](https://doi.org/10.1051/0004-6361/202140951)
- Chen, A. M., Takata, J., Yi, S. X., Yu, Y. W., & Cheng, K. S. 2019, A&A, 627, A87, doi: [10.1051/0004-6361/201935166](https://doi.org/10.1051/0004-6361/201935166)
- Chen, H.-Y., Gu, W.-M., Fu, J.-B., et al. 2022, arXiv e-prints, arXiv:2208.08972. <https://arxiv.org/abs/2208.08972>
- Chernyakova, M., Malyshev, D., Mc Keague, S., et al. 2020, MNRAS, 497, 648, doi: [10.1093/mnras/staa1876](https://doi.org/10.1093/mnras/staa1876)
- Chernyakova, M., Neronov, A., Lutovinov, A., Rodriguez, J., & Johnston, S. 2006, MNRAS, 367, 1201, doi: [10.1111/j.1365-2966.2005.10039.x](https://doi.org/10.1111/j.1365-2966.2005.10039.x)
- Chernyakova, M., Malyshev, D., van Soelen, B., et al. 2021, Universe, 7, 242, doi: [10.3390/universe7070242](https://doi.org/10.3390/universe7070242)
- CHIME/FRB Collaboration, Andersen, B. C., Bandura, K., et al. 2019, ApJL, 885, L24, doi: [10.3847/2041-8213/ab4a80](https://doi.org/10.3847/2041-8213/ab4a80)
- CHIME/FRB Collaboration, Andersen, B. C., Bandura, K. M., et al. 2020a, Nature, 587, 54, doi: [10.1038/s41586-020-2863-y](https://doi.org/10.1038/s41586-020-2863-y)
- CHIME/FRB Collaboration, Amiri, M., Andersen, B. C., et al. 2020b, Nature, 582, 351, doi: [10.1038/s41586-020-2398-2](https://doi.org/10.1038/s41586-020-2398-2)

- Connors, T. W., Johnston, S., Manchester, R. N., & McConnell, D. 2002, *MNRAS*, 336, 1201, doi: [10.1046/j.1365-8711.2002.05850.x](https://doi.org/10.1046/j.1365-8711.2002.05850.x)
- Cruces, M., Spitler, L. G., Scholz, P., et al. 2021, *MNRAS*, 500, 448, doi: [10.1093/mnras/staa3223](https://doi.org/10.1093/mnras/staa3223)
- Dai, S., Feng, Y., Yang, Y. P., et al. 2022, arXiv e-prints, arXiv:2203.08151. <https://arxiv.org/abs/2203.08151>
- Dai, Z. G., & Zhong, S. Q. 2020, *ApJL*, 895, L1, doi: [10.3847/2041-8213/ab8f2d](https://doi.org/10.3847/2041-8213/ab8f2d)
- Dubus, G. 2013, *A&A Rv*, 21, 64, doi: [10.1007/s00159-013-0064-5](https://doi.org/10.1007/s00159-013-0064-5)
- Gu, W.-M., Yi, T., & Liu, T. 2020, *MNRAS*, 497, 1543, doi: [10.1093/mnras/staa1914](https://doi.org/10.1093/mnras/staa1914)
- Hessels, J. W. T., Spitler, L. G., Seymour, A. D., et al. 2019, *ApJL*, 876, L23, doi: [10.3847/2041-8213/ab13ae](https://doi.org/10.3847/2041-8213/ab13ae)
- Hilmarsson, G. H., Michilli, D., Spitler, L. G., et al. 2021, *ApJL*, 908, L10, doi: [10.3847/2041-8213/abdec0](https://doi.org/10.3847/2041-8213/abdec0)
- Ho, W. C. G., Ng, C. Y., Lyne, A. G., et al. 2017, *MNRAS*, 464, 1211, doi: [10.1093/mnras/stw2420](https://doi.org/10.1093/mnras/stw2420)
- Ioka, K., & Zhang, B. 2020, *ApJL*, 893, L26, doi: [10.3847/2041-8213/ab83fb](https://doi.org/10.3847/2041-8213/ab83fb)
- Johnston, S., Ball, L., Wang, N., & Manchester, R. N. 2005, *MNRAS*, 358, 1069, doi: [10.1111/j.1365-2966.2005.08854.x](https://doi.org/10.1111/j.1365-2966.2005.08854.x)
- Johnston, S., Manchester, R. N., Lyne, A. G., et al. 1996, *MNRAS*, 279, 1026, doi: [10.1093/mnras/279.3.1026](https://doi.org/10.1093/mnras/279.3.1026)
- Josephy, A., Chawla, P., Fonseca, E., et al. 2019, *ApJL*, 882, L18, doi: [10.3847/2041-8213/ab2c00](https://doi.org/10.3847/2041-8213/ab2c00)
- Kashiyama, K., & Murase, K. 2017, *ApJL*, 839, L3, doi: [10.3847/2041-8213/aa68e1](https://doi.org/10.3847/2041-8213/aa68e1)
- Katz, J. I. 2021a, *MNRAS*, 501, L76, doi: [10.1093/mnras/slaa202](https://doi.org/10.1093/mnras/slaa202)
- . 2021b, *MNRAS*, 502, 4664, doi: [10.1093/mnras/stab399](https://doi.org/10.1093/mnras/stab399)
- . 2022, *MNRAS*, 510, L42, doi: [10.1093/mnras/slab128](https://doi.org/10.1093/mnras/slab128)
- Kochanek, C. S. 1993, *ApJ*, 406, 638, doi: [10.1086/172475](https://doi.org/10.1086/172475)
- Krtićka, J. 2014, *A&A*, 564, A70, doi: [10.1051/0004-6361/201321980](https://doi.org/10.1051/0004-6361/201321980)
- Levin, Y., Beloborodov, A. M., & Bransgrove, A. 2020, *ApJL*, 895, L30, doi: [10.3847/2041-8213/ab8c4c](https://doi.org/10.3847/2041-8213/ab8c4c)
- Li, D., Bilous, A., Ransom, S., Main, R., & Yang, Y.-P. 2022, arXiv e-prints, arXiv:2205.07917. <https://arxiv.org/abs/2205.07917>
- Li, D., & Zanazzi, J. J. 2021, *ApJL*, 909, L25, doi: [10.3847/2041-8213/abeaa4](https://doi.org/10.3847/2041-8213/abeaa4)
- Li, D., Wang, P., Zhu, W. W., et al. 2021a, arXiv e-prints, arXiv:2107.08205. <https://arxiv.org/abs/2107.08205>
- Li, Q.-C., Yang, Y.-P., Wang, F. Y., et al. 2021b, *ApJL*, 918, L5, doi: [10.3847/2041-8213/ac1922](https://doi.org/10.3847/2041-8213/ac1922)
- Lorimer, D. R., Bailes, M., McLaughlin, M. A., Narkevic, D. J., & Crawford, F. 2007, *Science*, 318, 777, doi: [10.1126/science.1147532](https://doi.org/10.1126/science.1147532)
- Lu, W., Kumar, P., & Zhang, B. 2020, *MNRAS*, 498, 1397, doi: [10.1093/mnras/staa2450](https://doi.org/10.1093/mnras/staa2450)
- Luo, D., McCray, R., & Mac Low, M.-M. 1990, *ApJ*, 362, 267, doi: [10.1086/169263](https://doi.org/10.1086/169263)
- Lyutikov, M. 2017, *ApJL*, 838, L13, doi: [10.3847/2041-8213/aa62fa](https://doi.org/10.3847/2041-8213/aa62fa)
- Lyutikov, M., Barkov, M. V., & Giannios, D. 2020, *ApJL*, 893, L39, doi: [10.3847/2041-8213/ab87a4](https://doi.org/10.3847/2041-8213/ab87a4)
- Manchester, R. N., Johnston, S., Lyne, A. G., et al. 1995, *ApJL*, 445, L137, doi: [10.1086/187908](https://doi.org/10.1086/187908)
- Marcote, B., Nimmo, K., Hessels, J. W. T., et al. 2020, *Nature*, 577, 190, doi: [10.1038/s41586-019-1866-z](https://doi.org/10.1038/s41586-019-1866-z)
- Margalit, B., & Metzger, B. D. 2018, *ApJL*, 868, L4, doi: [10.3847/2041-8213/aaedad](https://doi.org/10.3847/2041-8213/aaedad)
- Martin, R. G., Tout, C. A., & Pringle, J. E. 2009, *MNRAS*, 397, 1563, doi: [10.1111/j.1365-2966.2009.15031.x](https://doi.org/10.1111/j.1365-2966.2009.15031.x)
- Mckinven, R., Gaensler, B. M., Michilli, D., et al. 2022, arXiv e-prints, arXiv:2205.09221. <https://arxiv.org/abs/2205.09221>
- Melatos, A., Johnston, S., & Melrose, D. B. 1995, *MNRAS*, 275, 381, doi: [10.1093/mnras/275.2.381](https://doi.org/10.1093/mnras/275.2.381)
- Metzger, B. D., Berger, E., & Margalit, B. 2017, *ApJ*, 841, 14, doi: [10.3847/1538-4357/aa633d](https://doi.org/10.3847/1538-4357/aa633d)
- Metzger, B. D., Margalit, B., & Sironi, L. 2019, *MNRAS*, 485, 4091, doi: [10.1093/mnras/stz700](https://doi.org/10.1093/mnras/stz700)
- Michilli, D., Seymour, A., Hessels, J. W. T., et al. 2018, *Nature*, 553, 182, doi: [10.1038/nature25149](https://doi.org/10.1038/nature25149)
- Miller-Jones, J. C. A., Deller, A. T., Shannon, R. M., et al. 2018, *MNRAS*, 479, 4849, doi: [10.1093/mnras/sty1775](https://doi.org/10.1093/mnras/sty1775)
- Moffat, A. F. J., & Robert, C. 1994, *ApJ*, 421, 310, doi: [10.1086/173648](https://doi.org/10.1086/173648)
- Murase, K., Kashiyama, K., & Mészáros, P. 2016, *MNRAS*, 461, 1498, doi: [10.1093/mnras/stw1328](https://doi.org/10.1093/mnras/stw1328)
- Negueruela, I., Ribó, M., Herrero, A., et al. 2011, *ApJL*, 732, L11, doi: [10.1088/2041-8205/732/1/L11](https://doi.org/10.1088/2041-8205/732/1/L11)
- Neronov, A., & Chernyakova, M. 2007, *Ap&SS*, 309, 253, doi: [10.1007/s10509-007-9454-3](https://doi.org/10.1007/s10509-007-9454-3)

- Nimmo, K., Hessels, J. W. T., Keimpema, A., et al. 2021, *Nature Astronomy*, 5, 594, doi: [10.1038/s41550-021-01321-3](https://doi.org/10.1038/s41550-021-01321-3)
- Niu, C. H., Aggarwal, K., Li, D., et al. 2022, *Nature*, 606, 873, doi: [10.1038/s41586-022-04755-5](https://doi.org/10.1038/s41586-022-04755-5)
- Okazaki, A. T., Nagataki, S., Naito, T., et al. 2011, *PASJ*, 63, 893, doi: [10.1093/pasj/63.4.893](https://doi.org/10.1093/pasj/63.4.893)
- Oostrum, L. C., Maan, Y., van Leeuwen, J., et al. 2020, *A&A*, 635, A61, doi: [10.1051/0004-6361/201937422](https://doi.org/10.1051/0004-6361/201937422)
- Pastor-Marazuela, I., Connor, L., van Leeuwen, J., et al. 2021, *Nature*, 596, 505, doi: [10.1038/s41586-021-03724-8](https://doi.org/10.1038/s41586-021-03724-8)
- Petroff, E., Hessels, J. W. T., & Lorimer, D. R. 2022, *A&A Rv*, 30, 2, doi: [10.1007/s00159-022-00139-w](https://doi.org/10.1007/s00159-022-00139-w)
- Piro, A. L., & Gaensler, B. M. 2018, *ApJ*, 861, 150, doi: [10.3847/1538-4357/aac9bc](https://doi.org/10.3847/1538-4357/aac9bc)
- Pleunis, Z., Michilli, D., Bassa, C. G., et al. 2021, *ApJL*, 911, L3, doi: [10.3847/2041-8213/abec72](https://doi.org/10.3847/2041-8213/abec72)
- Puls, J., Markova, N., Scuderi, S., et al. 2006, *A&A*, 454, 625, doi: [10.1051/0004-6361:20065073](https://doi.org/10.1051/0004-6361:20065073)
- Quataert, E., & Gruzinov, A. 2000, *ApJ*, 545, 842, doi: [10.1086/317845](https://doi.org/10.1086/317845)
- Rajwade, K. M., Mickaliger, M. B., Stappers, B. W., et al. 2020, *MNRAS*, 495, 3551, doi: [10.1093/mnras/staa1237](https://doi.org/10.1093/mnras/staa1237)
- Reig, P. 2011, *Ap&SS*, 332, 1, doi: [10.1007/s10509-010-0575-8](https://doi.org/10.1007/s10509-010-0575-8)
- Rivinius, T., Carciofi, A. C., & Martayan, C. 2013, *A&A Rv*, 21, 69, doi: [10.1007/s00159-013-0069-0](https://doi.org/10.1007/s00159-013-0069-0)
- Rybicki, G. B., & Lightman, A. P. 1979, *Radiative processes in astrophysics*
- Shannon, R. M., Johnston, S., & Manchester, R. N. 2014, *MNRAS*, 437, 3255, doi: [10.1093/mnras/stt2123](https://doi.org/10.1093/mnras/stt2123)
- Snow, T. P., J. 1981, *ApJ*, 251, 139, doi: [10.1086/159448](https://doi.org/10.1086/159448)
- Sridhar, N., & Metzger, B. D. 2022, *ApJ*, 937, 5, doi: [10.3847/1538-4357/ac8a4a](https://doi.org/10.3847/1538-4357/ac8a4a)
- Sridhar, N., Metzger, B. D., Beniamini, P., et al. 2021, *ApJ*, 917, 13, doi: [10.3847/1538-4357/ac0140](https://doi.org/10.3847/1538-4357/ac0140)
- Tendulkar, S. P., Gil de Paz, A., Kirichenko, A. Y., et al. 2021, *ApJL*, 908, L12, doi: [10.3847/2041-8213/abdb38](https://doi.org/10.3847/2041-8213/abdb38)
- Tong, H., Wang, W., & Wang, H.-G. 2020, *Research in Astronomy and Astrophysics*, 20, 142, doi: [10.1088/1674-4527/20/9/142](https://doi.org/10.1088/1674-4527/20/9/142)
- Usov, V. V., & Melrose, D. B. 1992, *ApJ*, 395, 575, doi: [10.1086/171677](https://doi.org/10.1086/171677)
- Wada, T., Ioka, K., & Zhang, B. 2021, *ApJ*, 920, 54, doi: [10.3847/1538-4357/ac127a](https://doi.org/10.3847/1538-4357/ac127a)
- Wang, F. Y., Wang, Y. Y., Yang, Y.-P., et al. 2020, *ApJ*, 891, 72, doi: [10.3847/1538-4357/ab74d0](https://doi.org/10.3847/1538-4357/ab74d0)
- Wang, F. Y., & Yu, H. 2017, *JCAP*, 2017, 023, doi: [10.1088/1475-7516/2017/03/023](https://doi.org/10.1088/1475-7516/2017/03/023)
- Wang, F. Y., Zhang, G. Q., Dai, Z. G., & Cheng, K. S. 2022a, *Nature Communications*, 13, 4382, doi: [10.1038/s41467-022-31923-y](https://doi.org/10.1038/s41467-022-31923-y)
- Wang, P., Zhang, Y., Zhu, W., et al. 2022b, *The Astronomer's Telegram*, 15619, 1
- Waters, L. B. F. M. 1986, *A&A*, 162, 121
- Wei, Y.-J., Zhao, Z.-Y., & Wang, F.-Y. 2022, *A&A*, 658, A163, doi: [10.1051/0004-6361/202142321](https://doi.org/10.1051/0004-6361/202142321)
- Xiao, D., Wang, F., & Dai, Z. 2021, *Science China Physics, Mechanics, and Astronomy*, 64, 249501, doi: [10.1007/s11433-020-1661-7](https://doi.org/10.1007/s11433-020-1661-7)
- Xu, H., Niu, J. R., Chen, P., et al. 2022, *Nature*, 609, 685, doi: [10.1038/s41586-022-05071-8](https://doi.org/10.1038/s41586-022-05071-8)
- Yang, H., & Zou, Y.-C. 2020, *ApJL*, 893, L31, doi: [10.3847/2041-8213/ab800f](https://doi.org/10.3847/2041-8213/ab800f)
- Yang, Y.-P., Lu, W., Feng, Y., Zhang, B., & Li, D. 2022a, *ApJL*, 928, L16, doi: [10.3847/2041-8213/ac5f46](https://doi.org/10.3847/2041-8213/ac5f46)
- Yang, Y.-P., Xu, S., & Zhang, B. 2022b, arXiv e-prints, arXiv:2208.08712. <https://arxiv.org/abs/2208.08712>
- Yang, Y.-P., & Zhang, B. 2017, *ApJ*, 847, 22, doi: [10.3847/1538-4357/aa8721](https://doi.org/10.3847/1538-4357/aa8721)
- . 2018, *ApJ*, 868, 31, doi: [10.3847/1538-4357/aae685](https://doi.org/10.3847/1538-4357/aae685)
- Zanazzi, J. J., & Lai, D. 2020, *ApJL*, 892, L15, doi: [10.3847/2041-8213/ab7cdd](https://doi.org/10.3847/2041-8213/ab7cdd)
- Zdziarski, A. A., Neronov, A., & Chernyakova, M. 2010, *MNRAS*, 403, 1873, doi: [10.1111/j.1365-2966.2010.16263.x](https://doi.org/10.1111/j.1365-2966.2010.16263.x)
- Zhang, B. 2018, *ApJL*, 854, L21, doi: [10.3847/2041-8213/aaadba](https://doi.org/10.3847/2041-8213/aaadba)
- . 2020, *Nature*, 587, 45, doi: [10.1038/s41586-020-2828-1](https://doi.org/10.1038/s41586-020-2828-1)
- Zhao, Z. Y., & Wang, F. Y. 2021, *ApJL*, 923, L17, doi: [10.3847/2041-8213/ac3f2f](https://doi.org/10.3847/2041-8213/ac3f2f)
- Zhao, Z. Y., Zhang, G. Q., Wang, Y. Y., Tu, Z.-L., & Wang, F. Y. 2021, *ApJ*, 907, 111, doi: [10.3847/1538-4357/abd321](https://doi.org/10.3847/1538-4357/abd321)

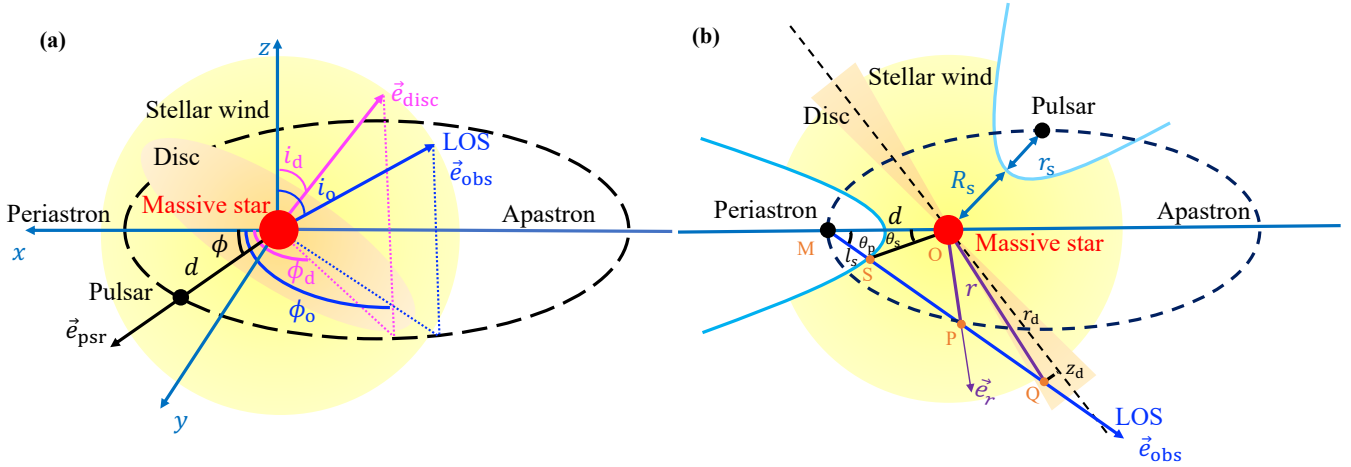


Figure 1. A schematic diagram of the pulsar/massive star binary (panel a, pulsar wind is not included) and the interactions between the smooth stellar outflows and the pulsar wind (panel b). The descriptions of parameters are given in Table 1.

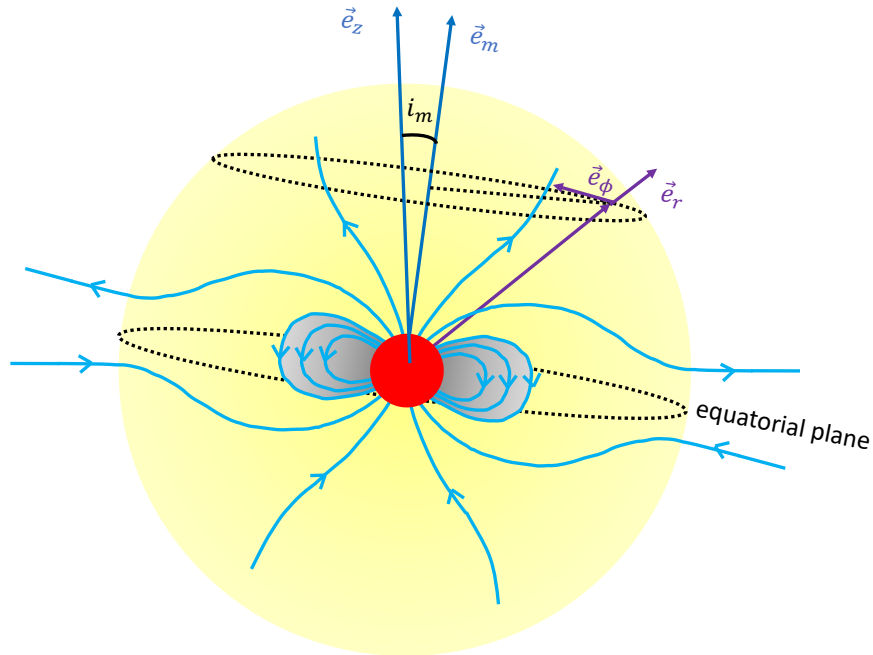


Figure 2. A schematic diagram of the magnetic field of a massive star. The orbital angular momentum is in the z -direction and the magnetic axis inclination angle is i_m . The magnetic field of the star is dipolar within the Alfvén radius R_A (shaded region). The magnetic field will become radial at a large distance because of the drag effect of the stellar wind and the fast rotation of OB stars will make the magnetic field become toroidal (Usov & Melrose 1992).

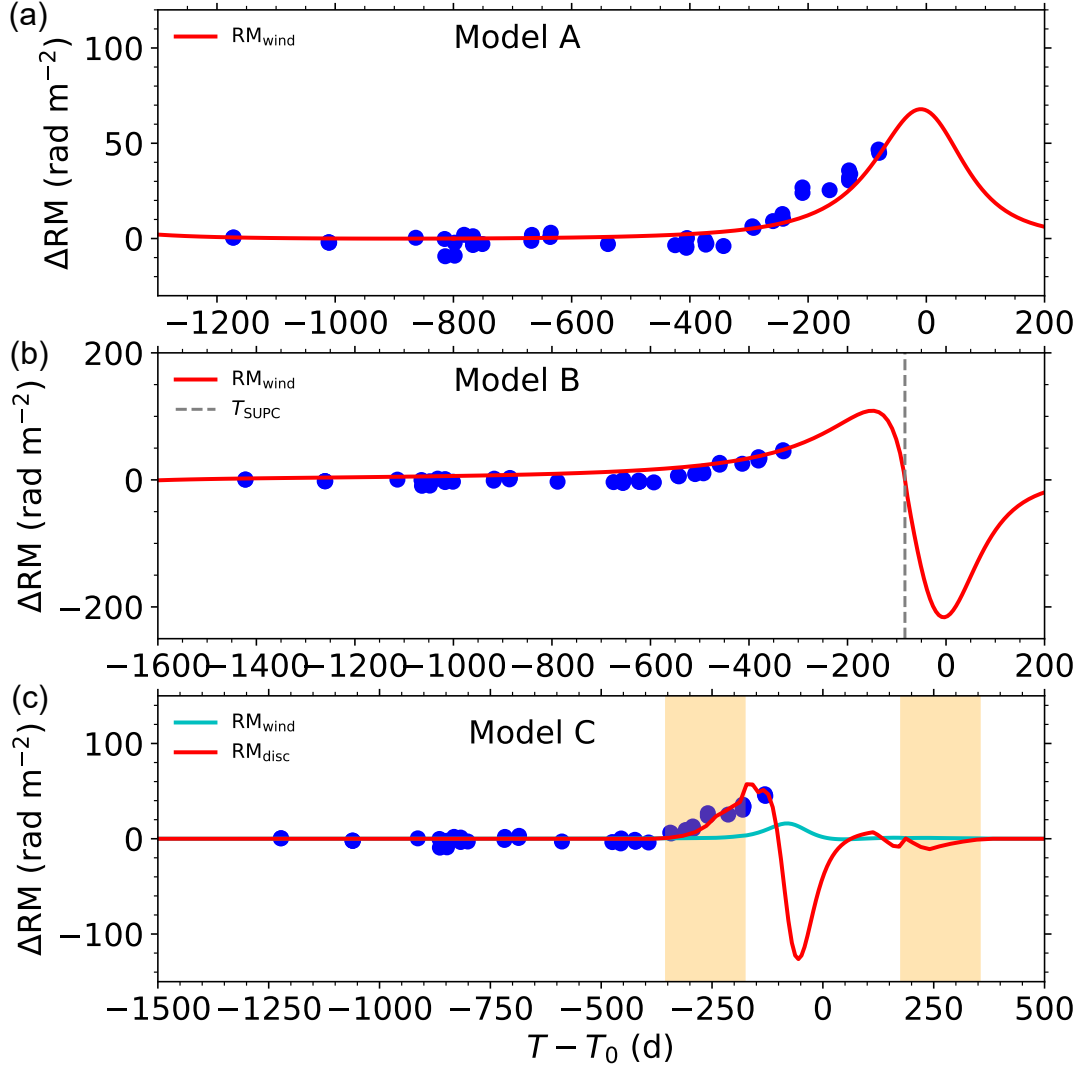


Figure 3. The RM variations from the stellar wind and disc. The blue circles represent the observed RM variations $\Delta\text{RM}_{\text{obs}} = \text{RM}_{\text{obs}} - \text{RM}_{\text{obs},0}$ from Mckinven et al. (2022), and $\text{RM}_{\text{obs},0} = -114 \text{ rad m}^{-2}$ is the value of the non-evolving phase (CHIME/FRB Collaboration et al. 2020b; Nimmo et al. 2021; Pastor-Marazuela et al. 2021; Mckinven et al. 2022). The fitting results are shown in solid curves, and the model parameters are listed in Table 2. (a): The fitting result of the radial magnetic field in the wind. Near periastron, RM variations reach the peak. (b): The fitting result of the toroidal wind magnetic field. RM will reverse before and after the SUPC ($T_{\text{SUPC}} = -83.4$ d). (c): The fitting result of the disc model and the contributions of the stellar wind is also considered. The toroidal magnetic field in the disc is used and the magnetic field in the stellar wind is assumed to be radial. The ΔRM from the disc and stellar wind is shown in red and cyan curves, respectively. The pulsar will pass through the inclined disc twice, i.e., before and after periastron. The orange-shaded regions represent the time when the pulsar passes through the disc. The pressure from the disc will reduce the momentum rate ratio of the pulsar and the stellar wind ($\sim 0.01\eta$). The radio signals travel through different components of the disc when a pulsar passes through the disc near periastron, which leads to complicated RM variations (e.g., with some minor structures and multiple reversals).

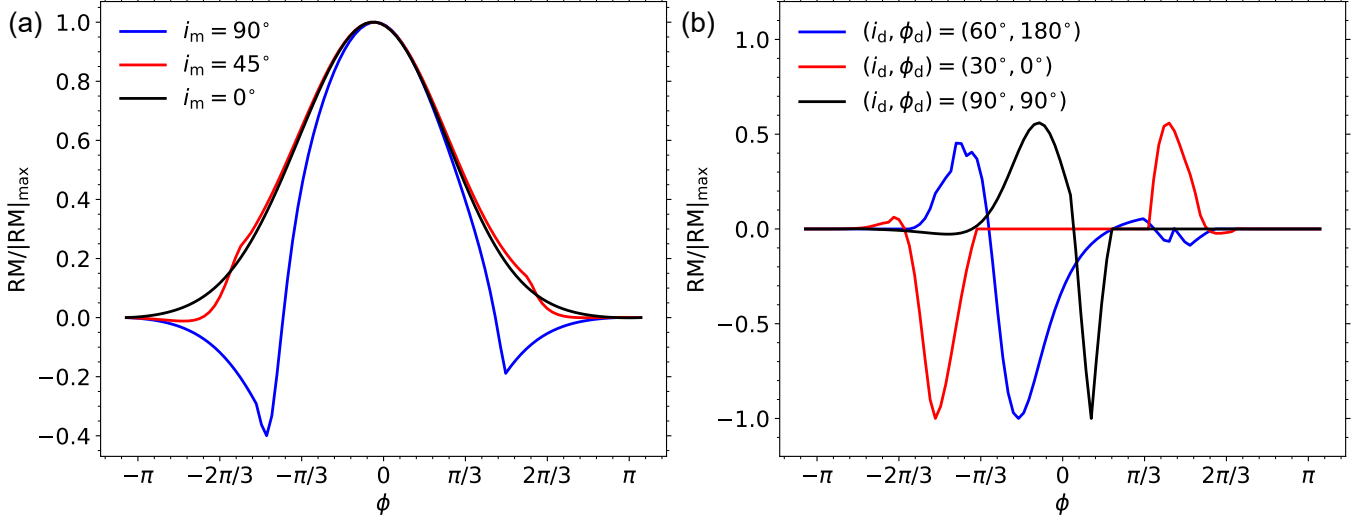


Figure 6. The orbital-dependent normalized RM of different magnetic axis inclination angles (panel a) and disc directions (panel b). (a) The wind magnetic field is radial and other parameters are the same as Model A. The RM does not reverse, except if the magnetic axis inclination angle is close to 90° . (b) The disc magnetic field is toroidal and other parameters are the same as Model C. RMs are complicated and profiles are completely different depending on the disc directions.

Table 1. Meanings and Typical Values of Physical Parameters in the model.

	Parameter	Symbol	Value	Reference
Star	Mass of star	M_\star	$30 M_\odot$	(1)
	Radius of star	R_\star	$\sim 10R_\odot$	(1,2)
	Effective temperature of star	T_\star	3×10^4 K	(1)
Stellar wind	Mass loss rate	\dot{M}	$10^{-11} - 10^{-8} M_\odot \text{ yr}^{-1}$	(3,4)
	Wind velocity	v_w	$3 \times 10^8 \text{ cm s}^{-1}$	(3,4)
	Wind temperature slope	β_w	$2/3$	(5,6)
Stellar disc	Disc density near stellar surface	$\rho_{d,0}$	$10^{-13} - 10^{-10} \text{ g cm}^{-3}$	(7)
	Disc density slope	β_d	3.5	(7,8)
	Inclination angle of the disc normal vector	i_d	60°	(9,10)
	True anomaly angle of the disc normal vector	ϕ_d	180°	(9,10)
	Half-opening angle	$\Delta\theta$	15°	(11)
Pulsar	Mass of pulsar	m	$1.4 M_\odot$	
	Spin-down luminosity	L_{sd}	$10^{35} - 10^{36} \text{ erg s}^{-1}$	(12,13)

References: (1) Negueruela et al. (2011); (2) Casares et al. (2005); (3) Snow (1981); (4) Krtićka (2014); (5) Kochanek (1993); (6) Bogomazov (2005); (7) Rivinius et al. (2013); (8) Carciofi & Bjorkman (2006); (9) Chen et al. (2021); (10) Martin et al. (2009); (11) Waters (1986); (12) Manchester et al. (1995); (13) Camilo et al. (2009);

Table 2. The model parameters of the RM fitting results for FRB 20180916B.

	Parameter	Symbol	Unit	Model A	Model B	Model C
	Period	P	d	1600	2000	16000
Orbital	Eccentricity	e		0.5	0.5	0.86
	Periastron time	T_0	MJD	59650	59900	59700
Observational	Inclination angle of observers	i_o		26°	154°	45°
angles	True anomaly angle of observers	ϕ_o		132°	132°	132°
Pulsar	Spin-down luminosity	L_{sd}	erg s^{-1}	10^{36}	10^{35}	10^{36}
	Mass loss rate	\dot{M}	$M_\odot \text{ yr}^{-1}$	10^{-8}	10^{-9}	10^{-8}
	Surface magnetic field	B_0	G	5	2	1
Stellar outflows	Wind magnetic field slope	α		2	1	2
	Disc magnetic field slope	α				1
	Disc density near stellar surface	$\rho_{d,0}$	g cm^{-3}			1.2×10^{-13}